FRACTURES OF THE FACIAL SKELETON

second edition

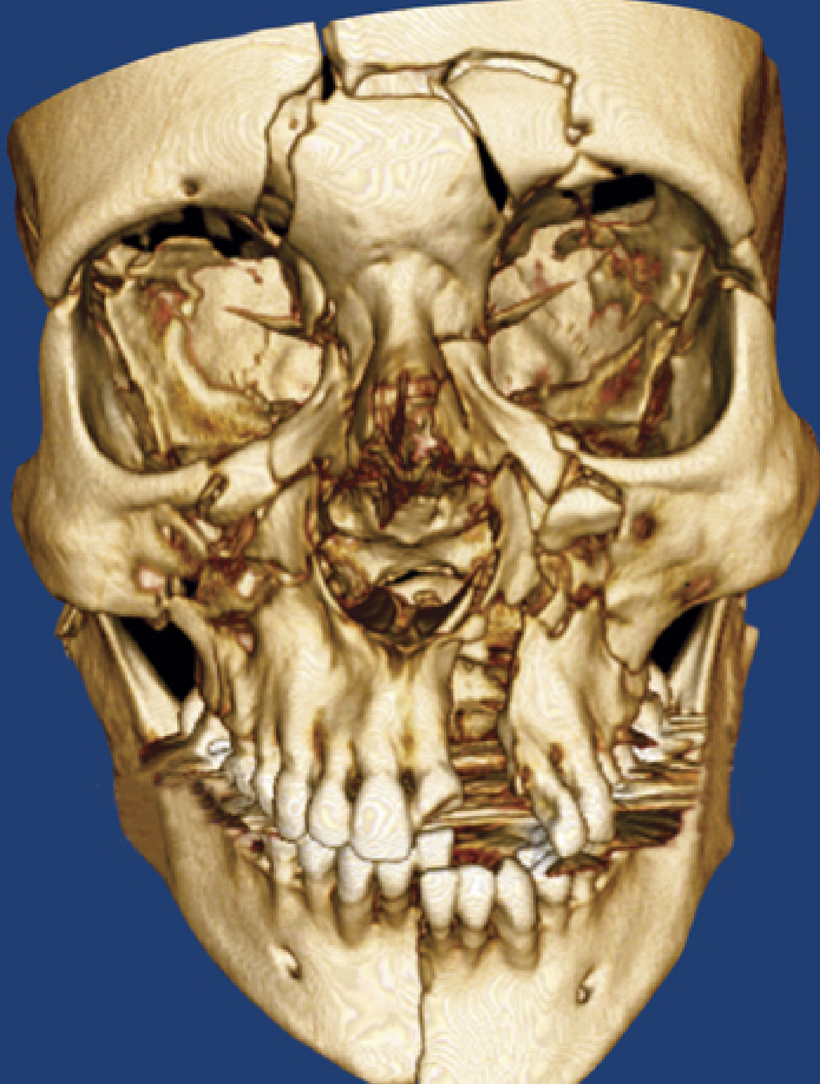

Michael Perry
Andrew Brown
Peter Banks

WILEY Blackwell

Table of Contents

List of Illustrations

laterally. The midline vomer is missing. (Courtesy of the Wellcome Museum of Anatomy and Pathology, Royal College of Surgeons of England.)

Figure 1.2 Diagrammatic representation of the relative strength of the skull and facial bones. The ‘matchbox’ like structure of the midface cushions the force of impact (B), whereas a blow to the skull is transmitted directly to the intracranial contents (A). An impact to the mandible (C) is transmitted indirectly to the cranial base. Damage to the brain may be prevented by protective fracture of the condylar neck, which is represented here as the handle of a bent baseball bat.

Figure 1.3 Transilluminated skull and facial bones demonstrating the thick buttresses of bone that distribute the forces of mastication within the skeleton of the midface. The much stronger bone of the mandible is also clearly evident. (Reproduced with kind permission of Springer Science+Business Media.)

Figure 1.4 View of the anterior cranial base showing the cribriform plate of the ethmoid with the olfactory nerve foramina and midline crista galli. This fragile bone is fractured in high midface Le Fort type and severe naso-orbito-ethmoid injuries. Damage to the underlying dura may result in cerebrospinal fluid rhinorrhoea.

Figure 1.5 The importance of accurate anatomical reduction to restore all three dimensions of the facial skeleton. Representation of a three-dimensional CT scan of a complex facial fracture that has been reduced and treated with miniplate fixation of the main buttress areas. (Reproduced with kind permission of Springer Science+Business Media.)

posterior attachment of the mylohyoid muscle, where bone contact is minimal.

Figure 2.4 The jaw thrust technique used to improve the airway in supine patients. The fingers are placed behind the angle of the mandible to push the jaw forwards and upwards while the thumbs push down on the chin or lower lip to open the mouth. Displacement of the mandible pulls the tongue forward and prevents occlusion of the oro-pharynx. In patients where there is no concern about any cervical injury the neck can be extended and the chin lifted to attain the same end. (John Wiseman, 1986.)

Figure 2.5 Nasopharyngeal airway tubes in place in a patient who has suffered a major facial injury. The ends of the tubes sit behind the tongue base in order to improve upper airway patency but regular aspiration is still mandatory to prevent blockage or pooling of blood and secretions. (Reproduced with kind permission of Springer Science+Business Media.)

Figure 2.6 Tracheostomy tube being inserted through a cricothyroidotomy incision. Note the use of tracheal dilator forceps to facilitate passage of the slightly smaller than normal tube through the cricothyroid membrane. (Reproduced with kind permission of Springer Science+Business Media.)

Figure 2.7 Postero-anterior cervical radiograph showing missing avulsed teeth identified in the oro-pharynx and upper trachea. Chest radiographs alone are inadequate when looking for missing teeth in the upper aerodigestive tract. (Reproduced with kind permission of Springer Science+Business Media.)

Chapter 3: Clinical features of facial fractures normal mode of treatment. When mandibular fractures are displaced it is usually as a result of the impact force stripping the periosteum and not muscle pull.

Figure 3.4 (a) Horizontally favourable and (b) horizontally unfavourable fractures of the left angle of the mandible. (See caption for Figure 3.3.)

Figure 3.5 Diagram to illustrate the mechanism of airway obstruction in an unconscious supine patient with posterior displacement of the symphysis. This is rarely a problem in a conscious patient even with significant injuries. In this situation the hyoglossus muscle and the intrinsic musculature, aided by the patient's upright posture, will allow control of the airway in almost all cases.

Figure 3.6 Occlusal disturbance produced by a unilateral displaced fracture of the left condylar neck. There is effective shortening of the ipsilateral ramus height leading to premature contact of the molar teeth. Deviation of the mandible to the affected side is also evident.

Figure 3.7 A young patient with bilateral displaced condylar neck fractures leading to an anterior open bite. In addition there is swelling over both fracture sites and painful limitation of all jaw movements.

Figure 3.8 Haematoma in floor of mouth as a result of an anterior mandibular fracture. This can be considered as a pathognomic sign of an underlying fracture when there is a clear history of an external blow.

Figure 3.9 Bilateral fracture of the parasymphysis with significant posterior displacement of the anterior mandibular segment. Despite this there was no evidence of airway embarrassment, demonstrating the innate ability of a conscious patient to maintain an airway in most situations. An unconscious supine patient would almost certainly obstruct with this type of injury.

Figure 3.10 Missile injury to the lower face and anterior mandible. Despite the loss of soft and hard tissue, and comminution of the remaining bone, the airway remained intact in this patient who was not rendered unconscious by his injury.

Figure 3.12 (a) Diagram to show how the orbital plate of the frontal bone and the sphenoid bone form an inclined plane which lies at approximately 45°to the occlusal plane. (b) In Le Fort II and III type fractures there may be infero-posterior displacement of the midfacial skeleton along this plane resulting in premature contact of the posterior teeth and an anterior open bite. Rarely, with extreme displacement, occlusion of the oral airway can occur due to retroposition of the soft palate. (c) More commonly, the complex of bones is comminuted on impact producing a 'dish-face' deformity with lengthening of the midface. This often gives the impression of greater posterior displacement than has actually occurred.

Figure 3.11 The classical lines of midface fracture as described by Le Fort (a) Frontal view, (b) Lateral view. *Red*: Le Fort I, Guérin or low level transverse fracture. *Blue*: Le Fort II, mid level pyramidal or infra-zygomatic fracture. *Green*: Le Fort III, high level transverse or supra-zygomatic fracture. Although this terminology has a venerable history in the maxillofacial literature modern imaging techniques confirm that injuries are usually considerably more complex than this ‘monobloc’ pattern suggests.

Figure 3.13 Patient with a high level midface fracture involving the cribriform plate with breach of the dura mater and cerebrospinal fluid (CSF) rhinorrhoea. The mixture of CSF (which does not coagulate) and blood (which does) results in a so-called ‘tramline’ pattern of discharge from the nose, as seen on the patient's left side. Note also the classical signs of a high level fracture including bilateral circumorbital ecchymosis (‘panda eyes’) and early gross facial swelling.

Figure 3.14 Superior orbital fissure syndrome due to fracture involving the left posterior orbit. (a) Paralysis and ptosis of upper eyelid. (b) Ophthalmoplegia with lack of movement of left eye in all positions of gaze (attempted downward gaze shown here). The patient also had anaesthesia of the left cornea and supra-orbital region. All these signs and symptoms usually resolve spontaneously with time.

Figure 3.15 Skull transilluminated from behind to show the relative strengths of the orbital bones. The extreme thinness of the floor and medial wall contrasts with the dense bone of the zygoma and orbital rim.

Figure 3.16 Typical zygomatic fracture lines. These rarely coincide exactly with the suture lines of the zygomatic bone, particularly medially, hence the more accurate terms ‘zygomatic complex fracture’ or ‘orbito-zygomatic fracture’. Note the usual proximity of the medial fracture line to the infraorbital foramen that explains the frequent finding of sensory loss over the cheek area and lateral nose.

Figure 3.17 Severe orbito-zygomatic injury with periorbital haematoma, flattening of the cheek, vertical separation of the frontozygomatic suture and consequent increase in orbital volume. The resulting enophthalmos, drop in position of the globe (hypoglobus) and pseudoptosis ('hooding') are obvious despite the swelling and haematoma.

Figure 3.18 Diagram illustrating possible locations of haemorrhage in the orbital area following trauma. 1. Lid ecchymosis. 2. Subperiosteal haematoma. 3. Haemorrhage posterior to the orbital septum (including subconjunctival haemorrhage). 4. Haemorrhage within the muscle cone (retro-bulbar haemorrhage). (Adapted from Soll (1977). Reproduced with permission of American Academy of Ophthamology and Otolaryngology.)

Figure 3.19 Diagram illustrating how inferior displacement of Whitnall's tubercle with the attached Lockwood's suspensory ligament leads to alteration in the level of the globe.

Figure 3.20 (a) Acrylic model produced from an impression of both orbital cavities viewed from above. Note that the medial walls are parallel whilst the lateral walls diverge at approximately 40–45° from the sagittal plane. (b) Oblique sagittal sections of both orbits as illustrated by red lines in (a). The normal sigmoid contour of the floor is demonstrated on the right. The typical loss of contour caused by a fracture involving the orbital floor is shown on the left. The stippled area represents the increase in orbital volume that results.

Figure 3.21 (a) Marked indentation of right cheek due to an isolated fracture of the zygomatic arch. (b)

Figure 6.2 Open reduction and internal fixation (ORIF) of a bilateral fracture of the mandible using an intraoral approach and titanium miniplates with monocortical screws. (a) Fracture of right angle fixed with a single plate adapted to lie along the upper border and external oblique ridge. (b) Left parasymphyseal fracture. In this area two plates are needed to achieve stable fixation. A temporary 'bridle wire' is visible in the upper part of the picture. This was placed around a number of firm teeth either side of the fracture in order to stabilize the reduction during application of the plates.

Figure 6.3 (a) Extra-oral approach used to treat a comminuted fracture of left mandible caused by a blow from a baseball bat. A rigid non-compression plate has been placed at the lower border. The head of a single lag screw inserted from the lower border across an oblique fracture can also be seen. (b) PA radiograph of reduced fracture with plate *in situ*.

Figure 6.4 Diagram to represent the theory of compression plating. During final tightening of the screw head in the eccentric pear-shaped hole (a) there is inward movement as it slides into the wider part and (b) thus pushes the bone fragments together.

Figure 6.5 Diagram illustrating the major problem with compression plating of the mandible. (a) A single plate near the lower border tends to open up the fracture at the alveolar level unless a 'tension band' is also placed; either (b) an arch bar or (c) a second smaller plate.

Figure 6.6 Diagram to illustrate the principle of lag screws. The thread only engages the deeper section of bone (a) and thus compression is applied as the screw is tightened (b).

Figure 6.7 Immobilization of a fractured mandible in a young patent by bonding small brackets onto teeth and applying intermaxillary fixation with orthodontic elastics.

Figure 6.8 Diagram illustrating the steps involved in the application of an eyelet wire.

Figure 6.9 Incorrect (a) and correct (b) method of tightening intermaxillary tie wires. Breakage is common if the wire is held in the forceps at right angles to the loop as it is pulled and twisted tightly. It is better to position the twisted portion close to an eyelet as shown to minimize sharp angulation of the wire.

Figure 6.10 Elastic 'guiding' IMF applied using modified eyelet wires. A few extra twists to the eyelet portion increases the length allowing them to be bent as a hook for the elastic band.

Figure 6.11 (a) Mandibular fracture treated with IMF using Jelenko pattern arch bars ligated to upper and lower teeth. (b) Models demonstrating the use of simple half-round arch bars. Small notches cut into the bars will prevent lateral slippage of the IMF wires. (Reproduced with kind permission of Springer Science+Business Media.)

Figure 6.12 IMF screw being inserted between the upper right canine and first premolar. Care is needed to avoid damage to the adjacent roots. If IMF screws are simply to be used for intraoperative stabilization they can sometimes be placed in the safer area beyond the apical region. However, difficulty of subsequent access and problems with ulceration preclude this location for longer term use. (Reproduced with kind permission of Springer Science+Business Media.)

Figure 6.13 One method of external fixation, used here for an infected fracture of the left mandible. Two screw pins have been inserted into each fragment and a length of endotracheal tube pushed over the protruding ends prior to the injection of self-curing acrylic resin. External fixation is rarely indicated and has been superseded in most situations by internal fixation techniques.

Figure 6.14 Lower border wiring. The reduced fracture has been stabilized by a direct interosseous wire and a separate ‘Figure of eight’ wire around the lower border. Although this technique has been superseded by the use of plates and has the added disadvantage of requiring an external approach it can still achieve excellent fixation. It may occasionally have a place in situations where plating equipment is not readily available.

Figure 6.15 Diagram illustrating the steps in a retromandibular approach to the mandibular condyle. (a) 1.5–2.0 cm vertical incision just behind the posterior border of the mandible. (b) The cutaneous incision is essentially parallel to the main lower division of the facial nerve and subsequent blunt dissection to reach the mandible avoids damage to this structure. (c) Wide subperiosteal dissection exposes the fracture site. (See text for details.)

Figure 6.16 (a) Direct fixation of right condylar neck fracture using a retromandibular approach. The patient is supine with the earlobe to the left of the picture. Note two plates in position to resist displacing forces. (b) A similar technique using a slightly more anterior transparotid dissection. (Reproduced with kind permission of Springer Science+Business Media.)

Figure 6.17 (a) Young patient who had sustained an intracapsular fracture of the left condyle some years previously. Note the smaller left hemi-mandible with deviation of the chin point to the left. This was associated with an increasing limitation in mouth opening. (b) Exposure of the left temporomandibular joint using a pre-auricular incision with a temporal extension. The condylar neck has been sectioned prior to removal of the deformed condylar head (arrowed). In this case the ankylosis was mainly fibrous.

Figure 6.18 Primary bone grafting to fracture of a thin edentulous mandible. (a) Displaced fracture of left body exposed. (b) Reduction and alignment with the help of a small miniplate. This is insufficient for effective stable fixation because the screws only engage lightly in thin and atrophic bone. (c) Segments of split rib graft applied to superior and inferior surface and held in place with tightly tied circum-mandibular polydioxanone resorbable sutures. (d) Postoperative OPT showing reduction and stabilization with the help of the rib graft (faintly visible at the lower border). Healing was uneventful.

Figure 6.19 In the past many fractures of the edentulous mandible were treated by closed reduction and fixation with the help of Gunnings type splints. These are no longer in common use but are illustrated here for historical interest. (a) Model demonstrating how splints are held in place with circum-mandibular and per-osseous wires. (b) Clinical application.

Chapter 7: Treatment of fractures of the midface and upper face eyelid region allows enough retraction to give wide exposure and the scar is essentially invisible. (Reproduced with kind permission of Springer Science+Business Media.)

Figure 7.7 An extended preauricular incision showing the exposure achieved for repair of fractures involving the left zygomatic arch and inferior aspect of the lateral orbital rim. (Reproduced with kind permission of Springer Science+Business Media.)

Figure 7.8 Diagram to illustrate various approaches to the inferior orbital rim using eyelid skin incisions. (a) Midtarsal incision with stepped post-orbicularis dissection. (b) Subciliary incision with pre-orbicularis dissection. (c) Subciliary incision with post-orbicularis dissection.

Figure 7.9 Transconjunctival approach to the inferior orbital rim. (a) Pre-septal dissection that minimizes herniation of orbital fat into the operative field. (b) Post-septal dissection that is considered technically easier.

Figure 7.10 Transconjunctival approach with lateral canthotomy for access to the inferior orbital rim and orbital floor. Note globe protection by insertion of a soft eye shell. (a) Insertion of scissors into the lateral fornix prior to division of skin and lateral canthus. (b) Conjunctiva being divided by scissors after undermining in the pre-septal plane along the marked incision line. (c) Elevation of the conjunctival mucosa with the help of traction sutures. (d) Incision of periosteum over the orbital rim and initial stages of elevation of the periorbita to expose the orbital floor. (e) Closure of lateral canthotomy skin incision with two fine resorbable sutures. (Courtesy of

zygomatic elevator (Bristow's) is inserted through an incision in the temporal fascia and passed superficial to the temporalis muscle to lie beneath the deep surface of the zygoma. (b) Clinical case using the same technique performed with a Rowe's elevator. (Reproduced with kind permission of Springer Science+Business Media.)

Figure 7.16 Depressed fracture of the left zygoma being elevated with the aid of a malar hook. The point of skin penetration is at the intersection of a horizontal line extending from the alar rim and a vertical line dropped from the lateral canthus. (Reproduced with kind permission of Springer Science+Business Media.)

Figure 7.17 Fixation of fractured zygoma with the aid of a buttress plate. This is a critical site to check the accuracy of reduction in order that any residual rotation or medial displacement are avoided. (Reproduced with kind permission of Springer Science+Business Media.)

Figure 7.18 Sagittal (a) and coronal (b) CT scans of an isolated orbital floor fracture with 'mirror image' superimposition of the normal side (purple). The alteration in the shape of the orbital floor and the extent of the increase in volume is obvious as shown by the arrows. (Courtesy of Jeremy Collyer, Queen Victoria Hospital, East Grinstead.)

Figure 7.19 Typical dimensions relevant to surgical exploration of the adult orbital floor. Mean distance from anterior lacrimal crest to the optic foramen = 42 mm. Distance from infraorbital foramen to inferior orbital fissure = 24 mm. The depth of the orbit is often unappreciated by less experienced surgeons who may not explore far enough posteriorly to

usually results in rounding of the arch (red) and loss of the normal straight profile (green). (b) Diagram showing how failure to correct this deformity in complex midface fractures will result in increased zygomatic width and postoperative flattening of the face.

Figure 7.26 The importance of medial canthal anatomy. (a) NOE fracture with flattening of the nasal bridge and infero-lateral displacement of the right medial canthus. (b) Restoration of canthal position after open reduction and fixation using a coronal flap for access.

Figure 7.28 Open reduction and fixation of NOE fracture with frontal bone involvement. Wide exposure allows full assessment of the injury with the best possibility of restoring the complex anatomy.

Figure 7.29 Diagram to illustrate the principle of transnasal canthopexy. (a) An awl or needle is passed through the nasal bones to pick up a braided wire suture attached to the canthal ligament. (b) The procedure may be combined with bone graft or titanium mesh reconstruction of the comminuted medial orbital wall. Even with these procedures post-traumatic canthal deformity is hard to prevent when the ligament has been completely detached.

Figure 7.30 CT scan showing fracture of posterior wall of left frontal sinus with an intact anterior wall.

Figure 7.31 (a) Depressed fracture of frontal bone causing obvious cosmetic deformity of forehead. (b) Coronal flap raised to expose fractures. (c) Reduction and fixation. In this case the repair was covered with acrylic bone cement to smooth out minor

identified in any laceration of this anatomical area. (Courtesy of Malcolm Cameron, Addenbrooke's Hospital, Cambridge.)

Figure 8.6 Full thickness laceration of upper lip involving the vermilion margin. (a) Wounds that involve key ‘margins’ (e.g. lip, nasal rim, ear or eyelid) require careful matching of anatomical landmarks. (b) In deep lip lacerations repair of the orbicularis muscle is also important. (Courtesy of Malcolm Cameron, Addenbrookes's Hospital, Cambridge.)

Figure 8.7 A crushed and contused wound of the scalp. Primary closure is not possible but a delay in treatment will allow any tissue of doubtful vitality to declare itself. With crush wounds healing by secondary intention or a skin graft may be indicated with revision surgery at a later date. (Perry (in press). Reproduced with kind permission of Springer Science + Business Media.)

Figure 8.8 (a) Shelving upper eyelid laceration. (b) Although quite deep with exposure of the orbital rim, repair was uncomplicated because the lid margin and the levator apparatus were not involved. Specialist referral is indicated for management of complex lid injuries. (Courtesy of Malcolm Cameron, Addenbrooke's Hospital, Cambridge.)

Figure 8.9 Missile injury to right face, neck and mandible. Gross comminution, wound contamination and a variable amount of tissue loss are features of this type of injury.

Figure 8.10 Shotgun injury resulting from an unsuccessful suicide attempt. Note the heavy contamination of soft tissues with fragmentation and